Int. J. Heat Mass Transfer. Vol. 36, No. 14, pp. 3565–3571, 1993
Printed in Great Britain

0017-9310/93 $6.00 + 0.00

Natural convection below heated horizontal rectangular plates

F. J. HIGUERA
E.T.S. Ingenieros Aeronáuticos Pza. Cardenal Cisneros 3, 28040 Madrid, Spain

(*Received* 14 *October* 1992)

Abstract—The boundary layer equations describing the high Grashof number laminar natural convection flow beneath a heated horizontal surface are solved numerically for an infinitely long strip with a uniform temperature central region and horizontal adiabatic extensions on the sides, and for rectangular plates of two different aspect ratios kept at constant temperature. The boundary condition required by these equations at the edge of the plate is discussed. The results are compared with existing approximate theoretical results and with experiments, as well as with the solutions obtained previously using the same method for a strip and a circular disk.

1. INTRODUCTION

CONVECTION induced by buoyancy below a finite size heated horizontal plate (or, equivalently, above a cooled plate) at high Rayleigh numbers is one of the basic classical problems in natural convection heat transfer. Experimental studies of this flow began with the works of Weise [1], Kraus [2], and Saunders *et al.* [3]. The first two works provided Schlieren photographs showing that the flow is directed from the centre toward the edges of the plate, and that the boundary layer thickness decreases in the same direction, whereas Saunders *et al.* measured the heat flux by optical means. Fishendon and Saunders [4] reported experiments with a heated square plate in air for Rayleigh numbers in the range 8×10^3–5×10^5 and fitted the Nusselt number to 1/4 to 1/5 power laws ($Nu \sim Ra^{1/4}$ to $Nu \sim Ra^{1/5}$). Kadambi and Drake [5] found a 1/5-power correlation for the laminar flow below a circular disk, and Birkebak and Abdulkadir [6] measured the temperature and velocity distributions in the boundary layer beneath a heated square plate submerged in water, finding the same power law correlation. Fujii and Imura [7] and Aihara *et al.* [8] used vertical side walls to create an approximately two-dimensional flow under the plate, and measured heat fluxes somewhat smaller than other experimenters; Fujii and Imura measured the heat flux in water for different plate inclinations, and Aihara *et al.* measured the temperature and velocity fields in air. Faw and Dullforce [9, 10] carried out measurements of the heat flux for downward facing square plates and disks using holographic interferometry. They found temperature distributions similar to the ones calculated by boundary layer theory.

Trying to ascertain the effect of the lateral sides of the plate, Restrepo and Glickman [11] evaluated the heat flux from measurements of the temperature profiles carried out for a square plate in air with heated and cooled vertical sides, and for a plate with horizontal adiabatic extensions. They reported variations of the order of thirty percent in the average Nusselt number, depending on the conditions at the edges. Hatfield and Edwards [12] obtained holographic interferograms for a range of Rayleigh numbers and adiabatic extensions.

It was early recognised that the outward boundary layer flow depends everywhere on the size and shape of the plate, so that: (i) no similarity solution of the kind found by Stewartson [13] for a heated semi-infinite upward facing plate (see also Gill *et al.* [14]) makes sense near the edge of a downward facing plate, and (ii) a boundary condition is required at the edge, which affects the upstream flow. Most of the theoretical work has been based on integral methods. Thus, using the integral method of Levy [15] and the condition that the boundary layer thickness vanishes at the edge (which is appropriate only for upward facing plates), Wagner [16] studied the two-dimensional flow below an infinite strip, and Singh *et al.* [17] extended this work to rectangular and circular plates. Singh and Birkebak [18] carried out computations for different Prandtl numbers using the alternative condition that the singularity appearing in the solution of the ordinary differential equations yielded by the integral method should occur at the edge. They found a finite boundary layer thickness there. Fujii *et al.* [19] proved that this latter condition is equivalent to the requirement that the boundary layer thickness at the centre of the plate should be minimum. Using somewhat different polynomial profiles, they performed computations for a strip, a circular disk, and a rectangular plate with uniform heat flux at the solid surfaces. Clifton and Chapman [20] recognised that the sudden relief of the constraint of horizontal motion imposed by the plate should be felt by the approaching flow, which should speed up as much as possible on reaching the edge. They translated this idea into a critical

NOMENCLATURE

b	aspect ratio of the rectangular plate
g	gravitational acceleration [m s^{-2}]
$\tilde{g}$	reduced gravity, $g\beta(T_w - T_\infty)$ [m s^{-2}]
Gr	Grashof number, $\tilde{g}L^3/\nu^2$
L	half-length of the shorter side of the plate [m]
Nu	average Nusselt number (equation (13))
p	dimensionless pressure
Pr	Prandtl number
s	length on the lateral surface [m]
T	temperature [K]
u, v	dimensionless x and y components of the velocity
u_c	characteristic velocity in the boundary layer [m s^{-1}]
w	dimensionless vertical (z) component of the velocity
x, y	dimensionless coordinates along the shorter and longer sides of the plate
z	dimensionless coordinate normal to the plate (downward).

Greek symbols

β	coefficient of thermal expansion [K^{-1}]
γ	extent of the heated area relative to the total area of the plate
δ_c	characteristic boundary layer thickness [m]
δ_1	dimensionless boundary layer thickness (equation (12))
θ	reduced temperature, $(T - T_\infty)/(T_w - T_\infty)$
λ	exponent in equation (10) determining the behaviour near the edge
ν	coefficient of kinematic viscosity [m^2 s^{-1}]
ξ, η	strained x and y coordinates (equation (11))
ρ	density of the fluid [kg m^{-3}]
φ	exponent in equation (11) determining the coordinate straining.

Subscripts

1	limiting conditions at the edge of the plate
w	conditions at the wall surface
∞	conditions far from the plate.

depth boundary condition for the boundary layer thickness at the edge, using an analogy with open channel hydraulics.

Goldstein and Lau [21] integrated numerically the full Navier–Stokes equations (without the boundary layer approximation) for the flow around an infinite strip at Rayleigh numbers ranging from 10 to 10^4. They considered both upward and downward facing surfaces with horizontal and vertical adiabatic extensions. They also carried out experiments with square naphthalene plates in air.

Schulenberg [22, 23] computed the local heat flux at the centre of an infinite strip and a circular disk at large and small Prandtl numbers using an approximate analytical method whereby the plate is first supposed to be immersed in an outer flow whose velocity is then determined using a condition of consistency with the buoyancy-induced velocity field.

Building upon the results obtained before for the asymptotic structure of the boundary layer near the edge [24], we analyse here the natural convection flow below a rectangular horizontal downward facing plate whose temperature is kept at a constant value T_w, higher than the temperature T_∞ of the surrounding fluid. We consider the limit of large Grashof numbers ($Gr = \tilde{g}L^3/\nu^2 \gg 1$, where $\tilde{g} = g\beta(T_w - T_\infty)$ and L is half of the length of the shorter side of the plate), in which several regions can be distinguished in the flow around the plate. The most important of these regions is the boundary layer beneath the plate, of characteristic thickness $\delta_c = O(L/Gr^{1/5})$, where the characteristic velocity of the flow is $u_c = O(\sqrt{(\tilde{g}L)}/Gr^{1/10})$. The horizontal flow in this boundary layer is driven by buoyancy in an indirect manner. Specifically, since the hydrostatic pressure distribution depends only on the local temperature distribution across the boundary layer, the pressure in the absence of any motion would be higher in the hot fluid beneath the plate than in the cold nearby fluid at the same depth but beyond the edge of the plate. This pressure difference pushes the fluid horizontally outward and, as a consequence, the heated layer becomes thinner near the edge than in the interior. This, in turn, gives rise to a nonuniform pressure distribution everywhere beneath the plate, with a pressure decreasing toward the edge, which sets the fluid into motion. Owing to the small thickness of the boundary layer, the vertical motion of the fluid in it is too weak to upset the aforementioned hydrostatic pressure balance, which persists when the flow is already established.

The restriction that the plate imposes on the vertical motion of the fluid ceases at the edge, and then, under the action of buoyancy, the fluid begins to move upward in a small region around the periphery of the plate. This is another of the characteristic regions of the present flow. An order of magnitude estimate shows that the incoming flow turns around the edge and acquires a vertical velocity of the order of its original horizontal velocity within a distance of order δ_c. This comparatively strong accelerating mechanism provided by buoyancy is able to deal with any flux supplied by the horizontal boundary layer, which means that the edge imposes no restriction at all on the horizontal boundary layer: the flow reaching the

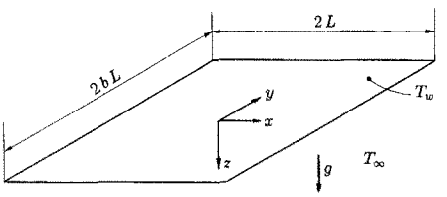

FIG. 1. Definition sketch.

edge will be as large as the indirect driving mechanism acting on the boundary layer permit. This is in keeping with the idea proposed by Clifton and Chapman, and was the basis of the asymptotic analysis of the boundary layer structure carried out in ref. [24].

2. FORMULATION

The equations describing the flow in the horizontal boundary layer (see Fig. 1) are

$$\frac{\partial u}{\partial x}+\frac{\partial v}{\partial y}+\frac{\partial w}{\partial z}=0, \tag{1}$$

$$u\frac{\partial u}{\partial x}+v\frac{\partial u}{\partial y}+w\frac{\partial u}{\partial z}=-\frac{\partial p}{\partial x}+\frac{\partial^2 u}{\partial z^2}, \tag{2}$$

$$v\frac{\partial v}{\partial x}+v\frac{\partial v}{\partial y}+w\frac{\partial v}{\partial z}=-\frac{\partial p}{\partial y}+\frac{\partial^2 v}{\partial z^2}, \tag{3}$$

$$\frac{\partial p}{\partial z}=-\theta, \tag{4}$$

$$u\frac{\partial \theta}{\partial x}+v\frac{\partial \theta}{\partial y}+w\frac{\partial \theta}{\partial z}=\frac{1}{Pr}\frac{\partial^2 \theta}{\partial z^2}, \tag{5}$$

where the horizontal distances x and y have been nondimensionalised with L; the horizontal velocities u and v with $\sqrt{(\tilde{g}L)}/Gr^{1/10}$; the vertical distance from the solid surface z (pointing downward) and the vertical velocity w with $L/Gr^{1/5}$ and $\sqrt{(\tilde{g}L)}/Gr^{3/10}$, respectively; the pressure (with the gravity term $-\rho_\infty gz$ included) with $\rho_\infty \tilde{g}L/Gr^{1/5}$; and the reduced temperature is defined as $\theta=(T-T_\infty)/(T_w-T_\infty)$.

The most characteristic feature of equations (1)–(5) is that the pressure is not known in advance, being determined by the flow itself. This gives an elliptic character to the problem, in such a way that the boundary conditions

$$u=v=w=\theta-1=0 \quad \text{at} \quad z=0, \tag{6}$$

$$u=v=\theta=p=0 \quad \text{for} \quad z\to\infty, \tag{7}$$

and the symmetry conditions

$$u=\frac{\partial v}{\partial x}=\frac{\partial \theta}{\partial x}=0 \quad \text{at} \quad x=0, \tag{8}$$

$$\frac{\partial u}{\partial y}=v=\frac{\partial \theta}{\partial y}=0 \quad \text{at} \quad y=0, \tag{9}$$

do not suffice to determine the solution, and must be supplemented with an additional condition at the edge of the plate ($x=\pm 1$ and $y=\pm b$; $b\geqslant 1$ being the plate aspect ratio).

In principle, the extra condition should come from the matching of the boundary layer and the turn around region at the periphery of the plate. It turns out, however, that the flow in the turn around region need not be studied in detail to obtain this condition, and the behaviour of the boundary layer near the edge can be found from a local analysis of (1)–(7) only. The results of this analysis, carried out in ref. [24], can be summarised as follows: matching with the strong acceleration occurring in the turn around region requires a large pressure gradient in the incoming boundary layer. With the scaling of the boundary layer, this pressure gradient tends to minus infinity at the edge (in the asymptotic limit $Gr\to\infty$). Then, under the action of a pressure gradient of increasing magnitude, the boundary layer nearing the edge split itself into a two-tiered structure. Transport effects are confined to a sublayer whose thickness tends to zero at the edge, whereas the flow outside this sublayer tends to a limiting state (denoted by the subscript 1 in what follows), being of the form

$$\{u,v,p,\theta\}=\{u_1(y,z),v_1(y,z),p_1(y,z),\theta_1(y,z)\}$$
$$+(1-x)^\lambda\{U(y,z),V(y,z),P(y,z),\Theta(y,z)\}+\cdots$$
$$w=(1-x)^{\lambda-1}W(y,z)+\cdots, \tag{10}$$

near the right end of the plate ($x=1$) (similar expressions hold in the rest of the periphery). Here, the limiting profiles depend to a large extent on the evolution of the flow upstream of the edge, whereas the exponent λ results from the matching with the transport sublayer, which is possible only for $\lambda\simeq 0.308$. We may note that λ determines the strength of the singularity of the normal derivatives of the velocity, pressure, and temperature at the edge. It is also worth noticing that upstream propagation of gravity waves in the stratified boundary layer becomes impossible under the conditions attained by the boundary layer immediately upstream of the edge. This fact points out the close analogy between the behaviour (10) and the choking conditions often found for compressible pipe flow: when (10) holds the flow beyond the edge can no longer influence the boundary layer because upstream information propagation becomes impossible.

Equations (10) provide the extra boundary condition for the boundary layer at the edge. To implement this condition in the numerical solution of the boundary layer problem, equations (1)–(5) were rewritten in terms of the strained coordinates

$$\xi=\frac{1}{2^\varphi}[(1+x)^\varphi-(1-x)^\varphi],$$

$$\eta=\frac{1}{(2b)^\varphi}[(b+y)^\varphi-(b-y)^\varphi], \tag{11}$$

so that, e.g. $\partial/\partial x=(\mathrm{d}\xi/\mathrm{d}x)\partial/\partial\xi$, with $\mathrm{d}\xi/\mathrm{d}x\sim 1/(1-|x|)^{1-\varphi}$ near the edge. Therefore, $1-\varphi$ is a meas-

ure of the strongest singularity effectively allowed when a condition of finite or zero ξ-derivative (obtained numerically by extrapolation) is imposed at $\xi = \pm 1$. This procedure will cope with the singularity (10) if a $\varphi < \lambda$ is chosen. Otherwise, φ is an artificial parameter, and the solution should not depend on it. This was checked for the results presented below by repeating the computations with different values of φ. Finally, $\varphi = 1/5$ was used for the two-dimensional computations of Section 3 and $\varphi = 1/4$ for the three-dimensional computations of Section 4.

For the numerical treatment, equations (1)–(9), rewritten in terms of (ξ, η, z), were discretised using centred differences in z, upwind differences for the ξ and η derivatives in the convection terms, and centred differences for the pressure terms. The discrete equations were solved with a pseudo-transient method. Results of the computations for an infinite strip and a circular disk can be found in ref. [24]. Here we consider the flow under an infinite strip with adiabatic extensions (Section 3) and under a rectangular plate for two different aspect ratios (Section 4).

3. HORIZONTAL STRIP WITH ADIABATIC EXTENSIONS

To simulate the effect of horizontal adiabatic extensions on the two-dimensional flow under a strip (b infinite), the boundary condition (6) for the temperature was changed to $\theta = 1$ at $z = 0$ for $|x| < \gamma$ and $\partial\theta/\partial z = 0$ at $z = 0$ for $\gamma < |x| < 1$. The value $\gamma = 0.8$ corresponds to one of the cases considered by Hatfield and Edwards [12], and $\gamma = 0.6$ is close to the 0.583 of Restrepo and Glickman [11].

The nondimensional shear stress and boundary layer thickness for $\gamma = 0.4$, 0.6 and 0.8, and $Pr = 0.7$, are shown in Fig. 2, and the results for an isothermal plate ($\gamma = 1$) have been included for comparison. The nondimensional boundary layer thickness is defined as

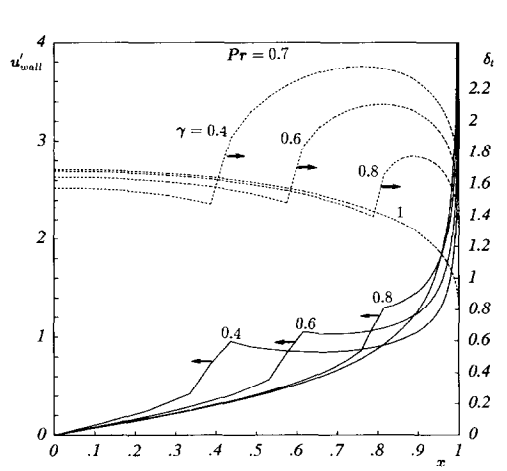

FIG. 2. Shear stress and boundary layer thickness on the right half of a strip for several adiabatic extensions.

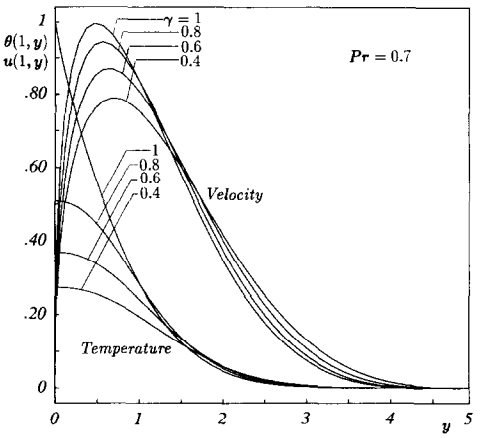

FIG. 3. Temperature and velocity profiles at the edge of the strip for several adiabatic extensions.

$$\delta_t = \frac{\int_0^z \theta \, dz}{\theta_{max}(x)}, \tag{12}$$

where $\theta_{max}(x)$ is the maximum temperature of the section.

The temperature and velocity profiles at the edge of the plate are represented in Fig. 3. The average values of the Nusselt number ($Nu = Gr^{1/5}\int_0^1 \theta_z \, dx$) for several γ's and $Pr = 0.7$ are given in Table 1.

As can be seen in Fig. 2, the shear stress increases around the point $x = \gamma$, and so does the local heat flux upstream of this point (not displayed). Beyond $x = \gamma$, the shear stress tends first to decrease (but still remains higher than for a uniform temperature plate over a substantial portion of the surface), and finally increases again near the edge, where the near-edge structure commented in Section 2 is retrieved. The boundary layer thickness presents a minimum at about $x = \gamma$. This was already noted by Restrepo and Glickman [11], who defined the thickness as the distance to the surface beyond which the temperature falls below a certain threshold. The increase of the thickness downstream of $x = \gamma$ is exaggerated by the definition used here, because θ_{max} is the temperature at the wall, which decreases very rapidly immediately downstream of $x = \gamma$, while the rest of the temperature profile changes more slowly with x. The apparent discontinuities in Fig. 2, specially for $\gamma = 0.4$, are an effect of the coarseness of the grid near the centre of the plate. Notice that downstream of $x = \gamma$ the pressure increases in the outermost region of the boundary layer, due to the increase of boundary layer thickness, but decreases in the bulk of the boundary layer, due to the decrease of temperature. This gives a large favourable pressure gradient at $x = \gamma$, which explains the large values of the heat flux and the shear stress at this point and a short distance upstream. The maximum of $-\partial p/\partial x$ at the wall occurs somewhat downstream of $x = \gamma$, at about the same position as the maximum shear stress, but $-\partial p/\partial x$ remains higher

Table 1. Average Nusselt numbers for several adiabatic extensions ($Pr = 0.7$)

γ	0.2	0.3	0.4	0.5	0.6	0.7	0.8	0.9	1
$Nu/Gr^{1/5}$	0.098	0.137	0.173	0.206	0.237	0.279	0.315	0.361	0.412

than for an isothermal plate a long distance beyond its maximum.

4. RECTANGULAR PLATES

Results of the numerical computations for rectangular plates are presented in Figs. 4–7. The increasing lines in Fig. 4 give the average Nusselt number,

$$Nu = \frac{Gr^{1/5}}{b}\int_0^1\int_0^b \frac{\partial\theta}{\partial z}\,dx\,dy, \qquad (13)$$

divided by $Gr^{1/5}$, as a function of the Prandtl number for a square plate ($b = 1$) and a rectangular plate ($b = 2$). For comparison, the average Nusselt numbers for a strip (b infinite; dashed line) and a disk (dotted line) have been plotted in the same figure. To make the values of $Nu/Gr^{1/5}$ for a disk commensurate with the others, they were first evaluated using the radius as the characteristic length and then multiplied by $2/\pi^{1/2}$, which is the ratio of the radius of a circle to the half-length of the side of a square plate having

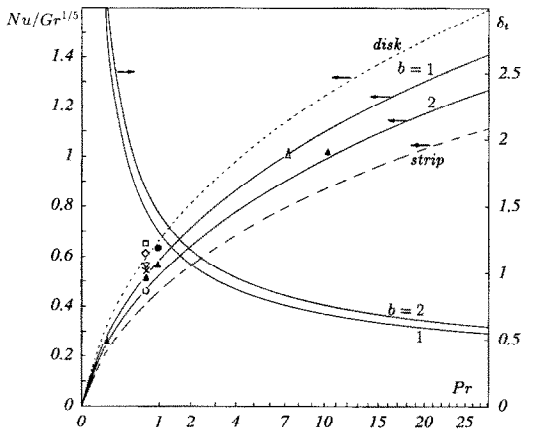

FIG. 4. Average Nusselt number for a square ($b = 1$) and a rectangular plate ($b = 2$), and boundary layer thicknesses at the centre of the plate, as functions of the Prandtl number. Dashed: Strip ($b = \infty$). Dotted: Circular disk. ○: Saunders *et al.* [3] ($b = 2$). ×: Restrepo and Glickman [11] ($b = 1$). ▽: Fishendon and Saunders [4] ($b = 1$). ◇: Faw and Dullforce [10] ($b = 1$). □: Weise [1] ($b = 1$). △: Birkebak and Abdulkadir [6] ($b = 1$). ●: Singh *et al.* [17] (theory; $b = 1$). ▲: Fujii *et al.* [19] (theory; $b = 1$).

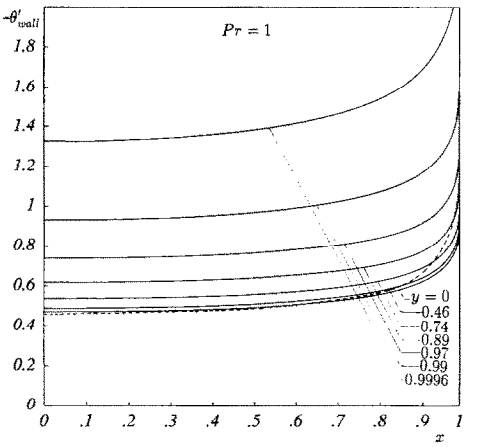

FIG. 6. Nondimensional heat flux along several lines parallel to the edge of a square plate for $Pr = 1$. Dashed: Results of ref. [17] (integral method) for $y = 0$.

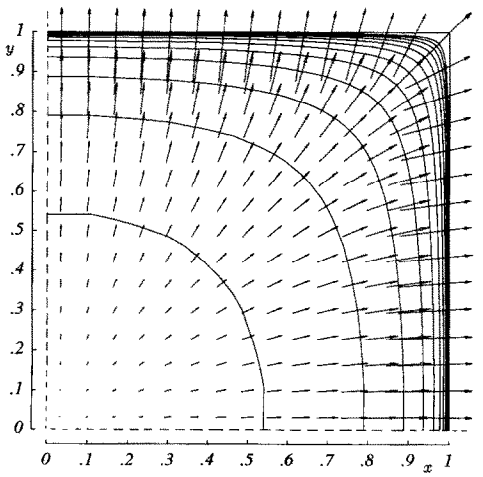

FIG. 5. Nondimensional heat flux (12 equi-spaced isolines between $\theta_r = 0$ and -1) and shear stress on the surface (arrows) on a quarter of a square plate for $Pr = 0.7$.

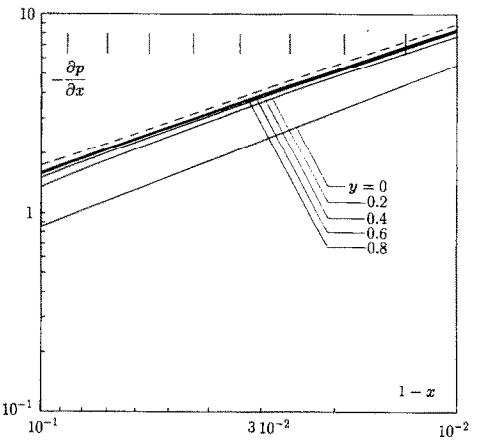

FIG. 7. x-Derivative of the pressure along lines of constant y near the right edge of a square plate for $Pr = 0.7$. The dashed line is the slope predicted by the asymptotic theory.

the same area; the re-scaling amounts to using the half-side of the equivalent plate as the characteristic length. Other theoretical and experimental values of the Nusselt number are also included in Fig. 4 for comparison. Even though the agreement is generally good, many of the experimental results are slightly higher than the theoretical prediction. This is probably an effect of the finite Grashof number not accounted for in the present boundary layer formulation; an explanation is given at the end of this section. On the contrary, the theoretical predictions of ref. [19], obtained with an integral method, are slightly lower than the present ones.

It was noted by Singh *et al.* [17] (see also [11, 23, 25], among others) that the circular disk and the infinite strip provide upper and lower bounds of the average Nusselt number for any reasonable shape of the plate, because, owing to geometrical reasons, they lead to minimal and maximal relative boundary layer thickness. This is confirmed by the present results. The decreasing lines in Fig. 4 represent the boundary layer thickness at the centre of the plate; the thicker boundary layer for the rectangular plate is in keeping with the aforesaid tendency.

The limits of small and large Prandtl numbers are specially interesting. In the asymptotic limit $Pr \ll 1$, heat conduction reaches farther away from the plate than viscosity. Hence, the effect of the viscous terms in (2) and (3) is negligible in most of the thermal boundary layer, and the balance of the remaining terms of (1)–(5) yields $z_c = O(Pr^{-2/5})$, which implies a nondimensional heat flux and average Nusselt number scaling as $Pr^{2/5}$. In the opposite limit, $Pr \gg 1$, fluid inertia is negligible in the thermal layer, and a similar balance with the left sides of (2) and (3) set to zero yields $z_c = O(Pr^{-1/5})$ and $Nu/Gr^{1/5} = O(Pr^{1/5})$. The numerical values $Nu/(Gr^{1/5}\, Pr^{2/5}) = 0.599$ (strip) and 0.895 (disk) for $Pr \to 0$, and $Nu/(Gr^{1/5}\, Pr^{1/5}) = 0.600$ (strip) and 0.862 (disk) for $Pr \to \infty$ were computed in ref. [24] by solving numerically the corresponding scaled boundary layer equations. (The values quoted for the disk correspond to having the lengths referred to $\pi^{1/2}/2$ times the radius). Although similar computations have not been carried out for rectangular plates, the results of Fig. 4 lend support to the assumption that these values would be intermediate between those of the strip and the disk.

Isolines of the nondimensional heat flux on one quarter of the surface of a square plate are given in Fig. 5 for $Pr = 0.7$. The arrows in this figure represent the shear stress on the plate. The accumulation of isolines near the edge is consistent with the divergence of the heat flux implied by (10). At a given point and constant b, the local nondimensional heat flux increases with Pr, owing to the decrease of the boundary layer thickness. On the contrary, the shear stress decreases with increasing Pr, because the decrease of the flow velocity offsets that of the boundary layer thickness. The distributions of heat flux and shear stress were compared in ref. [24] with other approximate results, obtained by integral methods, for the flows under strips and disks. Although similar detailed data are scarcer in the literature for rectangular plates, a comparison was carried out with the heat flux distribution given by Singh *et al.* [17] for a square plate and $Pr = 1$. The agreement was found to be good (see Fig. 6) in the central region of the plate, but gets worse near the edges, because of the erroneous assumption of zero boundary layer thickness used in ref. [17]. This situation is typical of many other theoretical and experimental approaches (see, e.g. Restrepo and Glickman [11] for a discussion of the sources of experimental error in the vicinity of the edge, or the discussion below on the influence of the flow outside of the boundary layer). These disagreements may or may not lead to discrepancies in the average Nusselt number, depending on whether the errors in the heat flux (which is itself higher near the periphery than at the centre of the plate) are offset by the reduced extent of the region where they occur.

Figure 7 is a logarithmic plot of the x-component of the pressure gradient near the right edge of the plate along six equispaced lines of constant y. (The vertical segments in the upper part of the figure give the locations of the grid lines). As can be seen, while the values of $-\partial p/\partial x$ are different for each y, the slopes tend to a common value, in accordance with the asymptotic results commented in Section 2. The dashed line in Fig. 7 has the slope $\lambda - 1 = -0.692$, given by the asymptotic analysis (equation (10)). The vertical shift of this line is arbitrary.

To estimate the influence of the flow exterior to the boundary layer, which is not taken into account at the leading order of boundary layer theory, let us consider the rather extreme case of a horizontal surface bounded by a vertical or appreciably inclined lateral surface extending upward from the edge and heated at a temperature comparable to that of the lower surface. The hot fluid near this lateral surface rises driven by the component of buoyancy tangential to the surface, moving with a velocity of order $\sqrt{(\tilde{g}s)}$ in a boundary layer of thickness $O(\nu^{1/2}s^{1/4}/\tilde{g}^{1/4})$, as results from standard estimates (see, e.g. ref. [25]; here s is the distance along the lateral surface measured from the edge). The entrainment rate of this lateral boundary layer is of order $\tilde{g}^{1/4}\nu^{1/2}/s^{1/4}$, which becomes $O(\sqrt{(\tilde{g}L)}/Gr^{1/4})$ at distances from the edge of order L. Since the entrainment of the horizontal layer is only of order $\sqrt{(\tilde{g}L)}/Gr^{3/10}$, the outer flow is controlled essentially by the suction of the lateral boundary layer. This suction is also felt inside the horizontal layer, where it adds to the outward flow, giving rise to velocities and heat fluxes higher than the ones predicted by present boundary layer analysis. The ratio of the entrainment-induced velocity to the characteristic horizontal velocity ($\sqrt{(\tilde{g}L)}/Gr^{1/10}$) is of order $Gr^{-3/20}$. Thus, although the effect of the outer flow is formally small (and the foregoing analysis is therefore valid), it can be quite appreciable for finite values of Gr of practical interest.

5. CONCLUSIONS

Natural convection high Grashof number flows below horizontal heated surfaces obey boundary layer equations. However, owing to the self-induced pressure gradient driving these flows, and to the outward-bound motion of the fluid, such equations have an elliptic character and require a boundary condition to be imposed at the edge of the plate. This condition expresses the matching of the boundary layer flow with the turn around region at the edge of the plate, where boundary layer theory is not applicable. The result is somehow analogous to the choking condition for compressible pipe flows, implying that the flow approaching the edge speeds up as much as it can before entering the turn around region, where even greater (upward) accelerations occur.

Using the above condition, the boundary layer problem has been solved numerically for rectangular plates kept at constant uniform temperature. Results are presented for two different aspect ratios and a range of Prandtl numbers, showing good agreement with other theoretical and experimental values. The present results confirm that the Nusselt number decreases with increasing plate aspect ratios, being maximum for a square plate, and that the values for any aspect ratio are bounded above and below by those of a circular disk and an infinite strip, respectively.

The effect of horizontal adiabatic extensions on a uniform temperature strip has also been analysed. The average Nusselt number is given for $Pr = 0.7$ and several lengths of the adiabatic extensions. The influence of the insulated regions on the boundary layer thickness and flow features has been discussed.

REFERENCES

1. R. Weise, Wärmeübergang durch frei konvektion on quadratischen platten, *Forsch auf Gebiet Ing.* **6,** 281–292 (1935).
2. W. Kraus, Temperatur- und geschwindigkeits feld bei konvektion um eine waagerechte quadratische platte, *Physik Zeits* **4,** 126–150 (1940).
3. O. A. Saunders, M. Fishendon and H. D. Mansion, Some measurements of convection by an optical method, *Engng* **139,** 483–485 (1935).
4. M. Fishendon and O. A. Saunders, *An Introduction to Heat Transfer*. Oxford University Press, London (1950).
5. V. Kadambi and R. M. Drake, Free convection heat transfer from horizontal surfaces for prescribed variation of surface temperature and mass flow through the surface, Tech. Rep. Mech. Engng HT-1. Princeton University (1960).
6. R. C. Birkebak and A. Abdulkadir, Heat transfer by natural convection from the lower side of a horizontal, heated surface, *4th Int. Heat Transfer Conf.*, Paris, Vol. 4, paper NC2.2 (1972).
7. T. Fujii and H. Imura, Natural-convection heat transfer from a plate with arbitrary inclination, *Int. J. Heat Mass Transfer* **15,** 755–767 (1972).
8. T. Aihara, Y. Yamada and S. Endo, Free convection along the downward-facing surface of a heated horizontal plate, *Int. J. Heat Mass Transfer* **15,** 2535–2549 (1972).
9. R. E. Faw and T. A. Dullforce, Holographic interferogrametry measurement of convective heat transport beneath a heated horizontal plate in air, *Int. J. Heat Mass Transfer* **24,** 859–869 (1981).
10. R. E. Faw and T. A. Dullforce, Holographic interferogrametry measurement of convective heat transport beneath a heated horizontal circular plate in air, *Int. J. Heat Mass Transfer* **25,** 1157–1166 (1982).
11. F. Restrepo and L. R. Glickman, The effect of edge conditions on natural convection from a horizontal plate, *Int. J. Heat Mass Transfer* **17,** 135–142 (1974).
12. D. W. Hatfield and D. K. Edwards, Edge and aspect ratio effects on natural convection from the horizontal heated plate facing downwards, *Int. J. Heat Mass Transfer* **24,** 1019–1024 (1981).
13. K. Stewartson, On the free convection from a horizontal plate, *Z. Angew. Math. Phys.* **9a,** 276–282 (1958).
14. W. N. Gill, D. W. Zeh and E. del Casal, Free convection on a horizontal plate, *Z. Angew. Math. Phys.* **16,** 539–541 (1965).
15. S. Levy, Integral methods in natural convection, *J. Appl. Mech.* **22,** 515–522 (1955).
16. C. Wagner, Discussion on integral methods in natural convection flows by S. Levy, *J. Appl. Mech.* **78,** 320–321 (1956).
17. S. N. Singh, R. C. Birkebak and R. M. Drake, Laminar free convection heat transfer from downward-facing horizontal surfaces of finite dimensions, *Prog. Heat Mass Transfer* **2,** 87–98 (1969).
18. S. N. Singh and R. C. Birkebak, Laminar free convection from a horizontal infinite strip facing downward, *Z. Angew. Math. Phys.* **20,** 454–461 (1969).
19. T. Fujii, H. Honda and I. Morioka, A theoretical study of natural convection heat transfer from downward-facing horizontal surfaces with uniform heat flux, *Int. J. Heat Mass Transfer* **16,** 611–627 (1973).
20. J. V. Clifton and A. J. Chapman, Natural convection on a finite-size horizontal plate, *Int. J. Heat Mass Transfer* **12,** 1573–1584 (1969).
21. R. J. Goldstein and K.-S. Lau, Laminar natural convection from a horizontal plate and the influence of plate-edge extensions, *J. Fluid Mech.* **129,** 55–75 (1983).
22. T. Schulenberg, Natural convection heat transfer to liquid metals below downward facing horizontal surfaces, *Int. J. Heat Mass Transfer* **27,** 433–441 (1984).
23. T. Schulenberg, Natural convection heat transfer below downward facing horizontal surfaces, *Int. J. Heat Mass Transfer* **28,** 467–477 (1985).
24. F. J. Higuera, Natural convection below a downward facing horizontal plate, *European J. Mech. B* (in press).
25. B. Gebhart, Y. Jaluria, R. L. Mahajan and B. Sammakia, *Buoyancy-induced Flows and Transport*. Hemisphere, New York (1988).